The International Journal of
Robotics Research

Tele-impedance: Teleoperation with impedance regulation using a body-machine interface

Arash Ajoudani, Nikolaos G. Tsagarakis and Antonio Bicchi

Tele-impedance: Teleoperation with impedance regulation using a body–machine interface

Arash Ajoudani[1,2], Nikos Tsagarakis[2] and Antonio Bicchi[1,2]

Abstract

This work presents the concept of tele-impedance as a method for remotely controlling a robotic arm in interaction with uncertain environments. As an alternative to bilateral force-reflecting teleoperation control, in tele-impedance a compound reference command is sent to the slave robot including both the desired motion trajectory and impedance profile, which are then realized by the remote controller without explicit feedback to the operator. We derive the reference command from a novel body–machine interface (BMI) applied to the master operator's arm, using only non-intrusive position and electromyography (EMG) measurements, and excluding any feedback from the remote site except for looking at the task. The proposed BMI exploits a novel algorithm to decouple the estimates of force and stiffness of the human arm while performing the task. The endpoint (wrist) position of the human arm is monitored by an optical tracking system and used for the closed-loop position control of the robot's end-effector. The concept is demonstrated in two experiments, namely a peg-in-the-hole and a ball-catching task, which illustrate complementary aspects of the method. The performance of tele-impedance control is assessed by comparing the results obtained with the slave arm under either constantly low or high stiffness.

1. Introduction

Master–slave teleoperation systems for unstructured and hostile environments have been studied and applied for a long time, starting even before the emergence of robotics systems (Goertz et al., 1961). Earlier prototypes using position measurements from the human operator arm to be replicated by a rigid manipulator soon showed their limitations in dealing with interaction tasks in uncertain environments, due to high forces developing at contacts. The second generation of teleoperation systems therefore included means of feeding back to the operator information on the interaction forces between the slave robot and the remote environment. Although such bilateral teleoperation systems can outperform pure position-controlled ones, they require an active force display on the master side (e.g. an actuated exoskeleton), which imposes extra costs and discomfort for the operator. Furthermore, latencies in the communication channel between the master and slave robot may generate insufficient transparency or even stability issues in the bilateral teleoperation system (see e.g. Hannaford and Anderson, 1988; Imaida et al., 2004; Niemeyer and Slotine, 2004).

Despite the results and continuous improvements in the mechatronics and control of bilateral teleoperation systems (Hannaford and Anderson, 1988; Sheridan, 1993; Leung et al., 1995; Eusebi and Melchiorri, 1998), there are still many tasks in which stability and reduced transparency, if not mere cost of sensing and actuating reflected forces, prevents application of bidirectional teleoperation. Tasks which are normally performed by humans without difficulty such as drilling, reaming, chipping and many others with large uncertainly in the environment constraints, cannot yet be easily conducted.

Part of these problems are certainly related to the slave side, where rigid manipulator arms are used to replace the sophisticated, adaptively compliant structure of the human

[1] Interdepartmental Research Center 'E. Piaggio', Faculty of Engineering, University of Pisa, Pisa, Italy
[2] Department of Advanced Robotics, Italian Institute of Technology, Genoa, Italy

Corresponding author:
Arash Ajoudani, Department of Advanced Robotics, Italian Institute of Technology, Via Morego 30, 16163 Genoa, Italy.
Email: arash.ajoudani@iit.it

arm. This aspect of problem has attracted much attention, and is at least partly solved, either by modern impedance control schemes on advanced arm hardware (Albu-Schäffer et al., 2007a,b), or by passively adaptive joints (Bicchi and Tonietti, 2004; Tonietti et al., 2005; Jafari et al., 2011). A second, perhaps harder, roadblock is that we do not really know as yet just how to *choose* and program variable impedance in a flexible and effective enough way.

Indeed, humans have superior motor capabilities and skills which permit them to effectively modulate their motion/impedance in a smooth and efficient manner according to the task needs. The role of impedance regulation in increasing stability, accuracy and task readiness has been illustrated in many papers (Gomi and Osu, 1998; Osu and Gomi, 1999; Gribble and Ostry, 2000; Franklin et al., 2003; Gribble et al., 2003; Tsuji et al., 2004). Such skills are deemed to be directed by learned goal-oriented internal models of the external world (Kawato, 1999).

Behavioral studies of human motor skills give evidence of the existence of two independent mechanisms in central nervous system (CNS) (Franklin et al., 2003; Selen et al., 2005). The former appears to be carried out by selective changes in patterns of activations in individual muscles to generate task-oriented force generation, while the latter is conducted by co-contraction of muscle groups, with no endpoint force changes. In addition to independency of these two subsystems, it has been observed that force and impedance variations observed while maintaining posture in response to mechanical disturbances show a linear relation with muscular activation levels (Selen et al., 2005).

Toward the twofold purpose of resolving some of the limitations of existing bilateral teleoperation systems, and of better understanding and exploiting the human skills in impedance regulation in interaction tasks, in this paper we propose and investigate the concept of 'tele-impedance'. In our approach, a compound reference command is obtained from the operator's arm using a suitable human–machine interface (HMI), which we use as a means of appointing the pathway between learned internal models and the external device to be controlled. Thus, results in this paper may complement well work not only in classical teleoperation applications, but also in modern cooperative manipulation tasks involving, e.g., a human and a humanoid (Adorno et al., 2011; Billard and Grollman, 2011).

HMIs for teleoperation of robot arms have been the subject of much attention in recent years. Electroencephalography (EEG) signals, which reflect correlated synaptic activities caused by post-synaptic potentials of cortical neurons, are most often used in brain–machine interfaces as command sources for assisting, augmenting, or repairing human cognitive or sensory-motor functions (Mussa-Ivaldi and Miller, 2003; Millan et al., 2004). However, high-level computational costs and complexity of present processing algorithms in EEG decoding have limited their application to few, very specific areas in the robotics field (e.g. Millan et al., 2004).

As an alternative for low-dimensional control spaces, body-machine interfaces (BMIs) have been proposed (Gulrez et al., 2008), which allow for the incorporation of relatively low-level and easier-to-handle biological signals in robotic applications. As far as the kinematic and dynamic requirements of tasks performed by the human arm are concerned, electromyography (EMG) signals, which are formed by superimposed patterns of activations of involved motor units, have been the choice input in many rehabilitative and human–robot functionality coordination (Fukuda et al., 2003; Castellini and Van Der Smagt, 2009; Artemiadis and Kyriakopoulos, 2010; Howard et al., 2011). Easy accessibility, fast adaptivity and stability of EMG signals are other advantages which motivated our choice of adopting EMGs in the real-time control of our tele-impedance system.

EMG can be used for different purposes. Using very simple filtering and averaging techniques, EMG can be effectively used to infer muscle activation levels rather accurately. Applying sophisticated processing techniques to whole segments of EMG recordings, time-frequency features can be accurately extracted (see e.g. Fukuda et al., 2003). More recently, the tendency of segmental processing to produce lag and jitter, which can be detrimental in real-time teleoperation, has been overcome by means of lag-free EMG processing techniques (see e.g. Vogel et al., 2011).

EMGs can also be used to provide information on an arm or hand posture, which has been used, e.g., for classification of hand gestures (Fukuda et al., 2003; Castellini and Van Der Smagt, 2009) or arm movements (Vogel et al., 2011). Because EMGs directly relate to muscle forces and not positions, their use to infer arm positions has to be indirect. One way of extracting arm positions from muscle forces is to infer joint torques τ from EMGs, and integrate the forward dynamics of motion of the arm, using an estimated kinematic and dynamic model of the arm, e.g. in the general Lagrangian form $B(q)\ddot{q} + C(q,\dot{q})\dot{q} + G(q) + J^{\mathrm{T}}F_{ext} = \tau$. A second possibility is to disregard dynamics. Under the hypothesis that the arm is only subject to the gravity torque term $G(q)$, the configuration q can be extracted inverting the map $G(q) = \tau$. This can be done (wherever $\frac{\partial G}{\partial q}$ is not singular) through a careful identification of the weight distribution, possibly learned through experiments (Vogel et al., 2011). However, neither method could be used in our applications, because a change in the weight distribution (as, e.g., when the operator arm has to support an object's weight, as in a ball reception experiment discussed later), or external forces F_{ext} acting on the master's hand would completely alter the force-based position estimates.

Therefore, in the proposed tele-impedance control method we provide the robot with two separate references, i.e. a desired 3D endpoint position and a desired 3D endpoint stiffness, obtained in different ways. Corresponding to the high priority given in teleoperation systems to position referencing, our BMI uses accurate measurement of arm
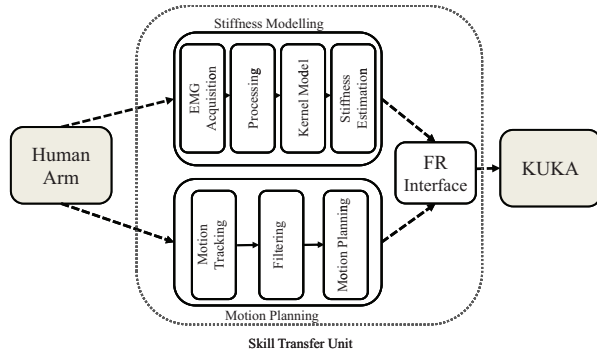
Fig. 1. The overall block diagram of tele-impedance.

position references through an unobtrusive optical tracking system. On the other hand, we process EMGs so as to separate the effects of endpoint force generation and stiffness variation, and use the latter as a reference for the robot impedance controller. The proposed control algorithm consists of controlling the slave robot using the accurate estimate of the master's position as the positional reference for the robot end-effector, around which an impedance controller is superimposed, for which references along different directions are provided by the processed EMG signals. The overall block diagram of tele-impedance control scheme is shown in Figure 1.

In this paper, we evaluate the efficiency of the proposed tele-impedance algorithm in two experimental tasks, illustrating different and complementary aspects of the method. The first concerns a classic peg-in-hole task, and is used to illustrate the stability, transparency and safety characteristics of the method. The second experiment, a ball-reception task, is chosen to assess how effective is the incorporation of human impedance regulation skills in performing tasks with significant dynamics. In both experiments, the slave robot performs the task by tracking both the reference position profile (which corresponds to the endpoint position of the arm of the human operator as measured from an optical position tracking system) and the endpoint stiffness profile (estimated from the muscular activities of the operator's arm) in real-time. Eventually, the performance of the proposed algorithm is compared with the behaviour of the robot arm with different constant stiffness settings.

Outline

Section 2 presents the model used to estimate human arm stiffness in 3D space. In Section 3 the experimental application of the proposed calibration method is presented and discussed. Section 4 discusses an application to a classical peg-in-hole task, while a ball-catching experiment is presented in Section 5.

2. Human arm impedance modeling in three dimensions

Contact reliability during tasks performed by humans in environments with stochastic uncertainties or while being exposed to mechanical disturbances can be ensured by a stable mechanical interface between human arm endpoint and the environment (Osu and Gomi, 1999; Burdet et al., 2001; Perreault et al., 2004). Quantification of this stability could be done by measurements of the visco-elastic profile of the human arm endpoint. Early studies conducted by Mussa-Ivaldi et al. (1985) demonstrated spring-like properties of human muscles. At around the same time, the human arm endpoint stiffness profile was estimated by means of imposed displacements and resulting steady-state force responses. Other studies analyzing the overall human arm impedance have also been carried out (Dolan et al., 1993; Tsuji et al., 1995; Gomi and Osu, 1998; Tsuji et al., 2004).

Perturbation-based impedance estimation techniques are currently the most accurate and reliable, due to direct measurements of the applied force–displacement profiles. However, their application can be problematic when real-time estimation of the human arm impedance is required during the execution of the task. As a consequence, current work is devoted to application of continuous and adaptive biosignals (e.g. EMGs) which correlate with human impedance modifications (Osu and Gomi, 1999). This work proposes a new method for the estimation of human arm endpoint stiffness, based on extraction of stiffness-related EMG features in real-time.

Task-oriented modifications of the endpoint arm stiffness along with endpoint force variations in humans are shown to have strong correlation with the patterns of activations in the involved muscles (Osu and Gomi, 1999; Franklin et al., 2003; Selen et al., 2005). Agonist–antagonist muscle co-contractions affect and modify selectively the overall stiffness and viscous profiles of the arm endpoint. Resulting modifications in force and impedance can be regarded as the effects of internal force regulation exerted by group of extensor and flexor muscles. It should also be noted that, when muscles act on multiple limb segments or about multiple axes of rotation (as is the case at the shoulder joint), the separation of muscles into agonist and antagonist can be oversimplifying, and a more general concept of muscle groupings or synergies should be considered (Turvey, 2007).

Based on this and the observed approximate linear dependency of force/stiffness to muscular activation/coactivations (Franklin et al., 2003; Selen et al., 2005), the overall mapping between muscular activities and resulting arm endpoint force and stiffness in Cartesian coordination and around equilibrium position (close to isometric condition) can be compactly described by

$$\left[\begin{array}{c} F \\ \sigma \end{array} \right] = \left[\begin{array}{c} T_F \\ T_\sigma \end{array} \right] P + \left[\begin{array}{c} 0 \\ \sigma_0 \end{array} \right], \qquad (1)$$

where $F, \sigma \in \mathbb{R}^3$ are the endpoint force and stiffness vectors, respectively, σ_0 is the intrinsic stiffness in relaxed conditions, and $P \in \mathbb{R}^n$ is the vector of muscular activities of the n considered muscles, as obtained from preprocessing EMG signals from electrodes applied on each muscle (details on the preprocessing are given in Section 3).

Ideally, a model for the estimation of endpoint force and stiffness values (in the vicinity of a specific arm configuration) from measured muscular activities could be obtained by identification of the elements of T_F and T_σ. To obtain an accurate experimental identification, two ingredients are necessary. First, precise measurements of 3D endpoint force F and stiffness σ are needed. Second, a rich and varied enough set of data samples should be generated by the subject. As a result of both these issues, while identification of the EMG-to-force map T_F is relatively easily done, accurately identifying the EMG-to-stiffness map T_σ is more difficult.

Owing to such limitations in the estimation of T_σ, Osu and Gomi (1999) proposed an algorithm for estimating the human arm stiffness which relies on identifying the map between muscular activities (as coded by EMGs) and joint torques (in formulas, $\tau = T_\tau P$, where T_τ is the EMG–to–joint torque map). In this work, the authors estimate T_τ by combining shoulder and elbow torques in the horizontal plane with measured activities of six involved muscles. The identification of $T_\tau \in \mathbb{R}^{2 \times 6}$ is based on an assumed structure of the type

$$T_\tau = \begin{bmatrix} c_1 & -c_2 & 0 & 0 & c_5 & -c_6 \\ 0 & 0 & c_3 & -c_4 & c_7 & -c_8 \end{bmatrix},$$
$$c_i > 0, \ i = 1, \ldots, 8 \qquad (2)$$

which corresponds to the anatomical arrangement of the six considered muscles. Here, c_i are constant gains which correspond to the mapping from muscular activities to the joint torques, identified by experiments. Authors then propose an index of muscular co-contraction around the joint (IMCJ, denoted here as L) that is evaluated as

$$L = |T_\tau| \ P,$$

where the absolute value of matrix T_τ is meant elementwise. Each element of $L \in \mathbb{R}^2$ is considered to be linearly related to the corresponding joint stiffness, i.e.

$$\sigma_i = m_i L_i + \sigma_{0,i}, \quad i = 1, 2$$

where the constants $m_i, \sigma_{0,i}$ are experimentally identified on the basis of stiffness measurements (Osu and Gomi, 1999; Osu et al., 2002).

It should be noted that the method relies upon the availability of an accurate estimate of joint torques, which cannot be measured directly, and have to be computed from measured endpoint forces through the arm Jacobian as $\tau = J^T F$. Results based on the above method have demonstrated good performance for 2D joint stiffness estimation even during small movements in the vicinity of the posture.

However, application of this method to our problem poses some challenges. In our system, we want to estimate the 3D Cartesian endpoint stiffness using measurements of the activation of $n = 8$ involved muscles acting at the shoulder and elbow. First, as observed by Weiss (1941), anatomy does not warrant the separation in agonists and antagonists at a ball joint, as 'any one of the muscles of the shoulder can be engaged in phase or antiphase with any other muscle' (Turvey, 2007). Furthermore, the use by Osu and Gomi (1999) of an estimate of the arm Jacobian has the disadvantage of introducing errors due to imperfect adherence of the double shoulder and elbow joints to simple lower pair kinematic models (Shin et al., 2009), and a strong dependency on the subject's limb proportions. In conclusion, the assumption of a structure of the type (2) for the EMG-to-force map $T_F \in \mathbb{R}^{3 \times 8}$ is not justified in our case. By the same token, no simple relation between the EMG-to-stiffness map $T_S \in \mathbb{R}^{3 \times 8}$ and $|T_F|$ can be expected to hold.

To overcome the limitations of applicability of the method of (Osu and Gomi, 1999) in our setting, we exploit the observation that in our experimental conditions the generation of forces can be considered to be decoupled from the regulation of stiffness. It is well known that in general endpoint impedance has three components, depending on posture, force and co-contraction, respectively. While the first two components may be large and even dominating (Milner, 2002) in a large enough range of variations, an ample literature reports the existence and independence of co-contraction contribution to stiffness (Akazawa et al., 1983; De Serres and Milner, 1991; Milner et al., 1995). Because in our experiments we only use small motions about a reference configuration for the arm and small endpoint force variations, it can be safely assumed that the control of forces and stiffnesses are decoupled. Accordingly, for the first-order linearized model (1), we consider a decomposition of the space of muscular activations $\mathcal{P} \ni P$ as the direct sum of a force-generating subspace $\mathcal{P}_F$ and the force-map null space $\mathcal{P}_k = \ker T_F$, i.e.

$$\mathcal{P} = \mathcal{P}_F \oplus \mathcal{P}_k.$$

By choosing a right-inverse T_F^R of T_F, i.e. any $n \times 3$ matrix[1] such that $T_F T_F^R = I$, we also affix a system of coordinates to these subspaces. In these coordinates, we can decompose the vector of muscular activations P in a force-generating component P_F and a null-space component P_k as

$$P = T_F^R T_F P + \left(I - T_F^R T_F\right) P \stackrel{\text{def}}{=} P_F + P_k.$$

The null-space component P_k contains information on the co-contraction component of stiffness generation. It is convenient to give an alternative description of P_k as follows. Let N_F denote a basis matrix for the kernel of T_F, and let $\lambda = N_F^+ P_k = QP$ be the coordinates in that basis of P_k,
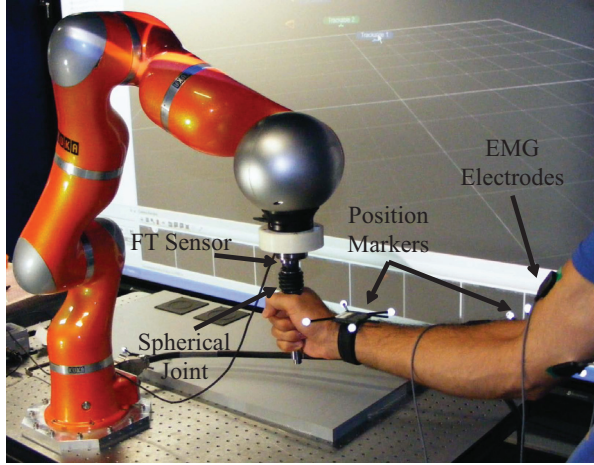
Fig. 2. Experimental setup used for the first calibration experiments. Subject applies constant forces in six directions while holding the handle attached to an idle spherical joint.

Fig. 3. Electrode positions in EMG measurements.

where $Q \stackrel{def}{=} N_F^+ \left(I - T_F^R T_F \right)$. Hence, the model of Cartesian stiffness regulation through co-contraction is written as

$$\sigma - \sigma_0 = M_\sigma Q P \qquad (3)$$

where $M_\sigma \in \mathbb{R}^{3 \times 5}$ is a mapping from the kernel of T_F (the set of muscle activations that do not change endpoint force, in the selected coordinate frame) to stiffness variations. The map M_σ can then be identified and calibrated once, based on direct measurements of human arm endpoint stiffness, at different co-activation levels as described in the following section. It is worth explicitly noting that the choice of the right-inverse T_F^R and that of the kernel basis N_F are both arbitrary, and imply an arbitrary description of the co-contraction component, for which only the calibration matrix M_σ is relevant. In other terms, there is no 'natural' choice of coordinates for $\mathcal{P}_k$, but, once one is given, this has to be used consistently for system calibration and operations.

Several caveats apply to the method for 3D stiffness estimation above, among which the fact that extrapolation of identified values of the maps to the whole workspace of the arm might not be valid, due to configuration dependency of human endpoint impedance and nonlinear dependency of the muscular activity and muscle tensions during movements. Also, large force variations would bring about stiffness changes of the same order or larger than co-contraction, thus violating the validity of the linearized model. However, as far as the tasks to be performed by the master arm remain in a vicinity of the static posture in which the parameters are estimated, and the human arm is not applying external forces, the approach provides a reasonable approximation of the endpoint stiffness profile in real-time.
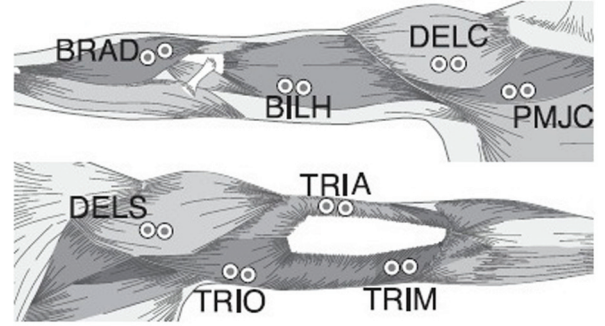
3. Stiffness model calibration–identification

3.1. Materials and methods

One healthy subject (male; age 27) participated in the identification–calibration experiments. The subject stood upright with the feet side by side in front of a robotic arm. The robot arm was equipped at the endpoint with a handle connected to a six-axis force and torque (F/T) sensor (ATI Mini-45). An idle spherical joint was used to connect the center of the handle to the F/T sensor, so as to avoid exertion of torques by the subject (see Figure 2). Displacements of the human arm at its endpoint (considered as the wrist center) were tracked by an Optitrack system (Natural Point, Inc.), with nominal resolution is 0.02 mm. Optical markers were also placed at the shoulder and elbow of the subject's arm. Both force and position measurements were acquired at a sampling frequency of 200 Hz, and filtered by a low-pass Butterworth filter with cutoff frequency 15 Hz to eliminate noise.

In all experiments, surface electromyograms (EMGs) were used to trace muscular activities. Eight dominant muscles acting on elbow and shoulder joints (see Table 1 and Figure 3) were chosen as the sources of EMG recordings. Analogue EMG signals were measured and amplified with a Delsys-Bangoli 16 (Delsys Inc.) apparatus. Acquired signals were band-pass filtered in the frequency range [20, 450] Hz. Resulting EMG signals were sampled at 2 kHz (PCI-6220, National Instruments) and fully rectified for further processing. A digital non-causal FIR linear phase low-pass filter was used for the detection of the envelope of the signal, which approximately corresponds to muscle activity.

The robotic arm is a seven-degree-of-freedom KUKA LWR with DLR's Fast Research (FR) interface (Schreiber et al., 2010). The data acquisition and synchronization interface between the KUKA controller, the EMG acquisition board, the Optitrack position streaming data and the six-axis F/T sensor were developed in C++.

3.2. Identification of the EMG-to-force map

In a first set of experiments, aimed at estimating the force-generating map T_F, the robot was only used passively, with

Table 1. Muscles used for EMG measurements.

Flexors		Extensors	
Monoarticular	Biarticular	Monoarticular	Biarticular
Deltoid clavicular part (DELC) Pectoralis major clavicular part (PMJC) Brachioradialis (BRAD)	Biceps long head (BILH)	Deltoid scapular part (DELS) Triceps lateral head (TRIA) Triceps medial head (TRIM)	Triceps long head (TRIO)

motors inactive and brakes turned on, serving only as a support structure for the F/T transducer mounted at the endpoint of the arm. The subject was asked to apply constant forces of ± 5 N, ± 10 N and ± 20 N, respectively, along six directions ($\pm x$, $\pm y$ and $\pm z$) while holding the handle (isometric conditions). Force components applied by the subject were measured and shown in real-time to the subject himself in the form of a graph with three colored bars on a screen. In each trial, the subject was instructed to apply forces so that bars reached and maintained given targets (corresponding in turns to the three different intensities in the three different directions). The subject was also instructed to use minimum muscular activity (minimum effort). Each trial was 60 seconds long. Data form the first 10 seconds were discarded to eliminate transient force fluctuations. For each direction and force level, four trials were executed and recorded (for an overall number of $4 \times 3 \times 2 \times 3$ trials) in the EMG-to-force map identification experiments. In a subsequent postprocessing phase, all components of (T_F) were evaluated by means of a least-squared-error algorithm, and a basis of its nullspace and the projector matrix Q used in (3) were computed.

3.3. Identification of the EMG-to-stiffness map

In a second set of experiments, aimed at estimating the stiffness-regulating map M_σ, similar equipment and arrangements were used. In this case, however, the robot was actively controlled and its Cartesian stiffness was set to the highest value possible (3 kN/m in all directions). To minimize voluntary stiffening behavior of the subjects arm, following Perreault et al. (2004) we applied continuous stochastic perturbations to the subject's hand through the handle in x, y and z directions. The amplitude of the applied perturbations had the peak-to-peak value of 20 mm in each direction. Figure 4 shows a typical applied endpoint displacements and restoring forces along x, y and z directions. Frequency spectrum of the perturbations were flat while decaying at the rate of 40 dB/Hz in frequencies higher than 4 Hz (Figure 5). This perturbation profile and corresponding forces in response, ensure adequacy of data for the identification of endpoint dynamics (Mann et al., 1989).

The experiments for EMG-to-stiffness map identification were performed by measuring the subject's force response to these random perturbations while the subject was instructed to set his arm's stiffness at a given
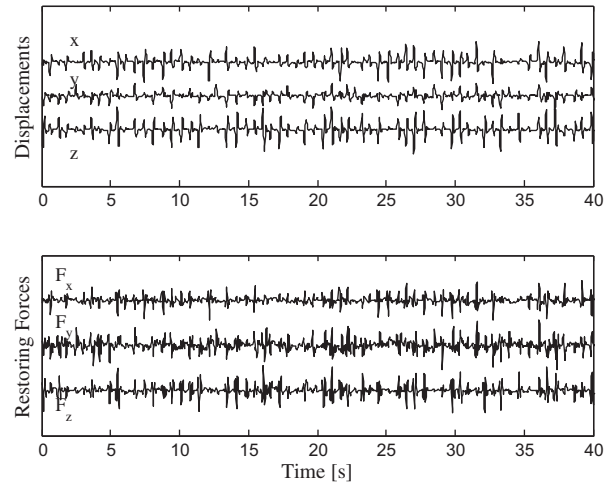

Fig. 4. Typical applied endpoint displacements and restoring forces in x, y and z directions. Each trial was 40 s long of which the last 35 s of the trials were used for the further processing.
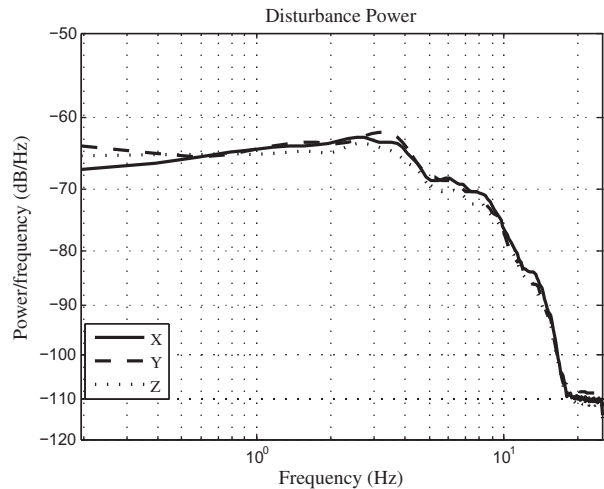

Fig. 5. Power spectrum of the applied disturbances.

level. Restoring forces exerted by the subject's arm were monitored by means of the F/T sensor, positions of the subject's wrist center were measured via the optical tracking system, and EMGs were acquired simultaneously and synchronously.

A rough stiffness indicator was graphically shown consisting of a bar of length proportional to the norm $|P|$ of the vector of muscle activations. Four different stiffness

reference levels were provided in different trials. The first set of random position perturbations was applied to the subject's hand at minimum muscle activity level (relaxed arm). The corresponding data was used to estimate the intrinsic stiffness σ_0 based on the identification protocol described below. Also, the endpoint inertia parameters in the vicinity of the predefined posture were identified in relaxed conditions, to be used later as a constant (under the simplifying assumption of negligible influence of muscle mass distribution on endpoint inertia) for the estimation of endpoint visco-elastic parameters in higher co-contraction trials. After such experiments in relaxed conditions, the subject was asked to stiffen his arm as hard as possible. The three reference levels of stiffness were hence defined by subdividing in four equal parts the measured interval of $|P|$ between its relaxed and maximum values.

Instructions given to the subject in the EMG-to-stiffness map identification phase included keeping the visualized index $|P|$ close to the set value during the experiment. Trials where the deviation from the preset level of $|P|$ were larger than 10% were discarded. Five successful trials were recorded for each level of arm stiffness. Each perturbation trial lasted 40 seconds. The first 5 seconds were used for allowing the subject to adapt to required stiffness level. The force on the handle caused by arm weight was removed as bias, being constant for small deviations from the equilibrium configuration.

The estimate of endpoint stiffness in different trials was performed based on measurement of corresponding pairs of forces and positions at the subject's wrist, following standard methods (see e.g. Perreault et al., 2004). For this reason, multiple-input, multiple-output (MIMO) dynamics of the endpoint impedance was decomposed into the linear subsystems associating each input to each output. Based on this assumption, and indicating with $F_x(f)$, $F_y(f)$ and $F_z(f)$ the Fourier transforms of the endpoint force along the axes of the cartesian reference frame, with $x(f)$, $y(f)$ and $z(f)$ the transforms of the human endpoint displacements, the dynamic relation between the displacements and force variations can be described by

$$\begin{bmatrix} F_x(f) \\ F_y(f) \\ F_z(f) \end{bmatrix} = \begin{bmatrix} G_{xx}(f) & G_{xy}(f) & G_{xz}(f) \\ G_{yx}(f) & G_{yy}(f) & G_{yz}(f) \\ G_{zx}(f) & G_{zy}(f) & G_{zz}(f) \end{bmatrix} \begin{bmatrix} x(f) \\ y(f) \\ z(f) \end{bmatrix}. \quad (4)$$

A non-parametric algorithm was adopted to identify the empirical transfer function of each of the single-input, single-output (SISO) subsystems described above in frequency domain (MATLAB, The MathWorks Inc.). The smoothed spectral estimates of input and outputs (using windowing techniques) were fed into this algorithm in order to identify each SISO transfer function. Consequently, we adopted a parametric, second-order, linear model of each impedance transfer function of the type

$$G_{ij}(s) = I_{ij}s^2 + B_{ij}s + K_{ij}, \quad s = 2\pi f\sqrt{-1}, \quad (5)$$

where I, B and K denote the endpoint inertia, viscosity and stiffness matrices, respectively. The parameters of the second-order linear model were identified based on a least-squares algorithm in the frequency range from 0 to 10 Hz. Although simple, this model has been shown to be adequate to the representation of the endpoint impedance of the human arm in a large class of tasks (Perreault et al., 2004; Tsuji et al., 2004).

Finally, in the postprocessing phase, experimental EMG vectors P were mapped in the EMG-to-force map nullspace through the previously computed projector matrix Q. The elements of the stiffness matrix K were used as estimates for the components of σ, and the map M_σ was estimated by applying a least-squared-error method to (3).

3.4. Identification results

The strength of linear dependency between measured force signals and estimates via the least-squared-error identification of the components of T_F was evaluated by Pearson's product-moment correlation coefficient. The coefficient is defined as

$$R_k = \frac{\sum \hat{f}_k f_k - \frac{\sum \hat{f}_k \sum f_k}{N}}{\sqrt{\left(\sum f_k^2 - \frac{(\sum f_k)^2}{N}\right)\left(\sum \hat{f}_k^2 - \frac{(\sum \hat{f}_k)^2}{N}\right)}}, \quad k = x, y, z, \quad (6)$$

where f_k and $\hat{f}_k$ are measured and estimated values of force in the Cartesian directions, and N is the number of pairs of data. The fit was consistently good in the three directions, resulting in average $R^2 = 81\%$. Figure 6 demonstrates the results of non-parametric and second-order model identification of the hand impedance transfer functions in the frequency range from 0 to 10 Hz, according to the methods described above. The second-order parametric impedance models presented (69.7%) of the data variance across all directions in minimum muscular activity trials in the frequency range of 0 to 10 Hz. Values of estimated endpoint inertia, damping and stiffness along the Cartesian directions are presented in Table 2. Estimated values are in good agreement with the former results of impedance estimation in two (Dolan et al., 1993; Tsuji et al., 1995) and three dimensions (Trumbower et al., 2009).

Extracting the symmetric and antisymmetric parts ($K_s = (K + K^T)/2$ and $K_a = (K - K^T)/2$, respectively) of the estimated stiffness matrix, it can be observed that the estimate is rather strongly symmetric ($\|K_a\|/\|K_s\| \approx 0.04$).

4. Validation in a peg-in-hole task

The efficiency of the tele-impedance approach to cope with contact stability issues is first evaluated in a peg-in-hole task, a classical benchmark for spatial planning with uncertainties.

The experiment was designed in order to explore the role of stiffness regulation during dynamic interaction between the peg and the hole, particularly its effect on the interaction

Table 2. Estimated hand impedance parameters.

Stiffness (N/m) K			Viscosity (Ns/m) B			Inertia (kg) I		
240.58	163.99	102.35	21.33	7.09	6.96	1.02	0.32	0.15
181.81	128.97	78.78	3.77	17.72	3.29	0.17	0.78	0.09
113.36	107.18	81.01	23.12	1.90	26.06	0.19	0.12	0.87
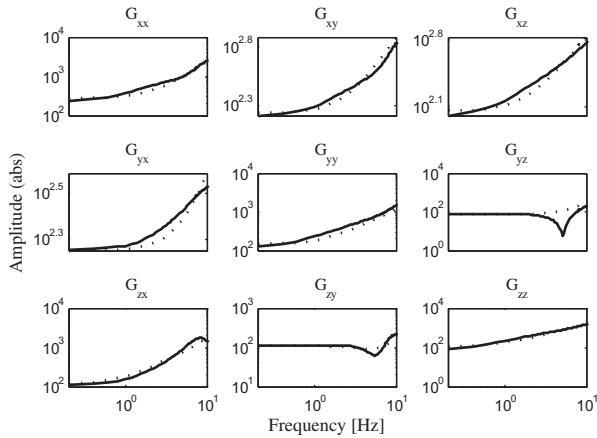
Fig. 6. Non-parametric (solid lines) and parametric second-order (dotted lines) transfer functions of SISO impedance subsystems obtained from stochastic perturbations.

forces. A reference configuration for the operator's arm was initially chosen so that he/she could perform the peg-in-hole task comfortably. Stiffness identification experiments were made in preparation for the experiment, in the same reference configuration for the human arm. Wrist, elbow and shoulder joint markers were used to gather arm postural data. In the actual experiment, the human operator was placed so that the slave endpoint frame was translated to the masters's own wrist frame laterally along the direction of the master's shoulder-to-shoulder line (y-axis). A geometric calibration was used to make sure that the reference human arm configuration corresponded to a robot's pose matching the hole position. In the experiment, the operator was allowed to start motion from an arbitrary position, was asked to move his/her hand to reach the reference configuration, and finally to teleoperate the robot to insert the peg in the hole. The master could see the slave arm, including the peg and hole. No peg was held by the master, nor did he receive any feedback except for seeing the slave arm operations. It should be noted that in the reaching phase, where stiffness calibration is not accurate, there are no interactions with the environment.

The experiment consisted of four parts. In the first part, the Cartesian stiffness of the slave endpoint was set to a relatively high, constant level ($K = [1,200, 1,200, 1,200]$ N/m) throughout the task. The second part was analogous, with low constant stiffness values ($K = [120, 120, 120]$ N/m). Third part concerns with the endpoint stiffness profile of the slave under constant and high along z and low

along x and y directions ($K = [250, 250, 1200]$ N/m). Values of high and low endpoint stiffness profiles were chosen based on human arm endpoint stiffness interval. The fourth part used variable impedance in the three directions, as derived from the proposed EMG processing method (tele-impedance control). Damping values in all experiments was set to a constant value of $D = [0.7, 0.7, 0.7]$ N.s/m. Further extensions of the method, providing the possibility of reproducing the off-diagonal stiffness terms and/or the endpoint damping behavior of the human with the slave robot arm (Tee et al., 2004), are possible but have not yet been demonstrated.

The experimental setup and information flow are shown in Figure 7. Body markers were attached to the wrist, elbow and shoulder of the human master's arm to track its motion. The reference trajectory calculation for robot motion was provided by the wrist marker, while the shoulder and elbow were used to make the final configuration of the master's arm coincide with the reference position, removing possible differences in the redundancy manifold. The robot base frame was considered as the overall reference frame for other frames (Optitrack and FT sensor). The position path of the human wrist was measured, low-pass filtered (cut-off 15 Hz) and used for trajectory planning. At the same time, EMG signals were acquired from the master arm and used to evaluate its endpoint stiffness based on the model and calibration described in the previous section. All processing and control algorithms were performed in real-time. Software interfaces, sampling frequencies, and hardware specifications are identical to those reported in the previous section.

The KUKA LWR's Fast Research Interface was used for commanding the position and Cartesian impedance controllers of the slave arm. Incremental position references were sent to the robot, calculated from the position tracking errors in three dimensions (7) as

$$e_{\mathrm{X}} = X_{\mathrm{human}} - X_{\mathrm{slave}} \qquad (7)$$

where e is the 3D tracking error vector between the reference Cartesian position vector of human wrist X_{human}, and the current Cartesian position vector of the robot end-effector, X_{slave}. This approach was used to cope with drift and tracking inaccuracy due to possible delays between reference commands and generated movement in the slave end-effector. The reconstructed values of the master arm stiffness were used as inputs for the robot endpoint impedance controller algorithm, described by Albu-Schäffer et al. (2007a,b) and implemented in the FRI.
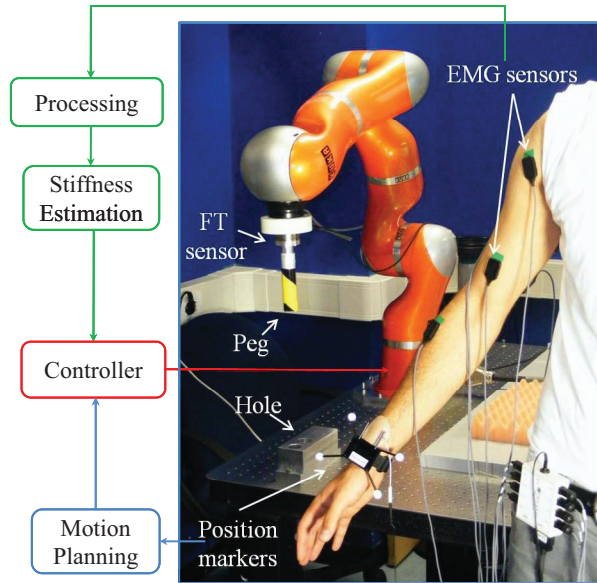
Fig. 7. Peg-in-hole experimental setup. KUKA light weight robotic arm, EMG electrodes, peg, hole, position tracking markers and F/T sensor are shown.

4.1. Experimental results

Figure 8 presents experimental results for the interaction forces between the peg and the hole, and the position tracking errors in three dimensions. As shown in Figure 8(a), when the slave arm is controlled to a constant high stiffness (equal to 1,200 N/m in all principal directions), the task could be successfully accomplished (see also Extension 1). However, even small position errors generated relatively large forces (up to 80 N in the negative z direction) at time $t = 10$ s when the interaction starts. This phenomenon indicates possible damaging effects both for the robot and for equipments/objects manipulated during the execution of the task.

Figure 8(b) demonstrates results from the second experiment, in which the task was executed with the slave arm stiffness fixed to low values (120 N/m in all principal directions). Position errors (particularly in the y direction) can be observed to be slightly increased in the reaching phase which is due to compliance of the robot leading to reduced dynamics and bandwidth. Once the peg is positioned close to the hole ($t \approx 18$ s), interaction forces raise to a value which is notably lower than in the former case. Small end-effector position adjustments, as a result of the master's hand movements, succeeded in aligning the peg with the hole ($t \approx 23$ s). After reaching the alignment, the master started the insertion phase by simply moving the hand down. An increase of the force in the vertical insertion direction can be consequently observed, which however is not sufficient to win friction forces between peg and hole and accomplish the task. As a consequence, the slave's end-effector could not track the subject's reference and position error increase, eventually reaching the slave arm controller's safety threshold and entering a fault condition ($t \approx 26$ s).

Figure 8(c) demonstrates typical results from third experiment. As depicted in the plots, even though the task is accomplished and interaction forces along the x and y directions between the peg and the hole surface are significantly reduced compared with first experiment, the algorithm still suffers from high interaction forces resulting from even very small position errors along the z direction, especially when the peg slides on the surface of the hole (from $t \approx 5.9$ s to $t \approx 8.6$ s).

Figures 9 and 10 demonstrate the experimental results obtained with application of tele-impedance control. In this experiment the operator guides the peg to the hole area keeping the arm in a natural, low-stiffness profile. In this phase, the arm is rather far from the posture where stiffness values were estimated, and calibration data obtained are invalid; however, in this phase position control is sufficient to guarantee good overall guidance in free space. Once the peg reaches to the reference configuration ($t \approx 12.5$ s), the operator begins moving his hand down towards the hole and exerting moderate forces. After some time (at $t \approx 17.5$ s), the master increases further his muscular activation to increase and adjust the endpoint stiffness (Figure 9) until a suitable level of stiffness is reached as to overcome friction. In this phase, the operator appears to be guided by a comparison of proprioception relative to his hand position, with visual feedback from the slave's endpoint. Finally, the operator moves his hand downwards until the peg is fully inserted into the hole. Similar stiffness levels were used to successfully pull the peg out from the hole ($t \approx 23$ s to $t \approx 25$ s). As depicted in Figure 10, both position tracking errors and interaction forces remain within acceptable levels, both in the search phase (between 13 s and 17.5 s, where high stiffness caused high interaction forces), and in the insertion phase (roughly between 17.5 s and 21 s, where low stiffness generated large tracking errors and ineffective forces). It should be noted again that the insertion and pull out phases were performed at a pose of the arm close to where the parameters of the endpoint stiffness model were estimated and calibrated.

5. Validation in a ball-catching task

Further evaluation of the proposed tele-impedance technique in conditions involving more significant dynamics was done through the execution of a ball-catching task. The task consisted of receiving a ball thrown at the arm's endpoint and bringing it to a stop in the reference position.

Two identical rigid balls ($m = 0.92$ kg, radius 52.5 mm) were suspended at the same distance above the human and robotic arm endpoints. The subject was prepared to receive the ball and instructed to hold his arm in a posture very close to that used during calibration experiments. The slave arm position, under gravity compensation, was in agreement. The balls were simultaneously dropped using a single manual release mechanism.
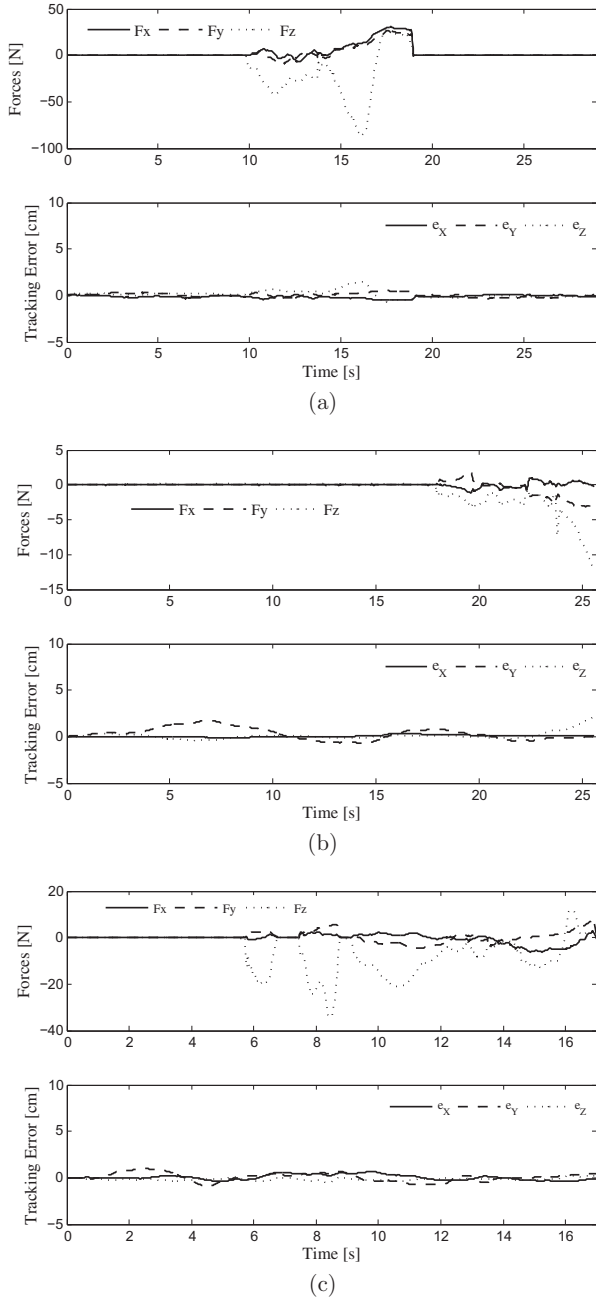
(a)

(b)

(c)

Fig. 8. Dynamic interaction forces between peg and the hole and position tracking error in the *x*, *y* and *z* directions, with (a) fixed high values of endpoint stiffness ([1,200, 1,200, 1,200] N/m), (b) fixed low values of endpoint stiffness ([120, 120, 120] N/m) and (c) fixed and high along the *z* and low along the *x* and *y* directions (*K* = [250, 250, 1,200] N/m).

The subject was instructed to receive the ball and stabilize its position back to the original arm's posture as smoothly and expediently as possible. The position of the slave endpoint was controlled along the master's wrist trajectory before and during catching, whereas the Cartesian stiffness values were controlled to constantly high, low or regulated to the master's stiffness level in three different
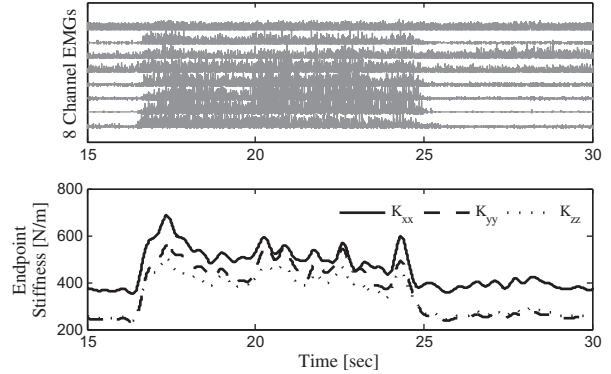

Fig. 9. Fully rectified eight-channel raw EMGs (upper plot) and estimated and mapped endpoint stiffness (lower plot) in real-time for the peg-in-hole task.
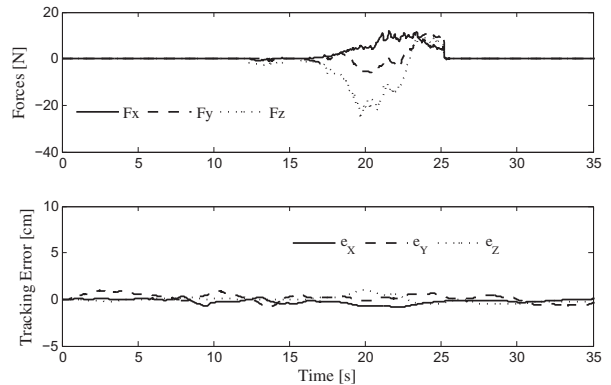

Fig. 10. Dynamic interaction forces between the peg and the hole (upper graph) and position tracking error in the *x*, *y* and *z* directions (lower graph) based on tele-impedance.

experimental phases, exactly as described in the previous section.

The experimental setup and information flow are shown in Figure 11. Software interfaces, marker placements, sampling frequencies, hardware specifications and calibration data were identical to those reported in previous sections.

5.1. Experimental results

Typical master's hand path in the *x*, *y* and *z* directions, and while performing the task are shown in Figure 12. These trajectories demonstrate the small range of required motion to perform the task and ensure the validity of the identified model in the reference posture.

The measured forces at the endpoint of the slave robotic arm during the task in the three stiffness control modes (constantly high, constantly low, and tele-impedance) are reported in Figure 13, while the corresponding deviation errors from the reference equilibrium position are in Figure 14. The regulation of the human arm muscle activations and resulting endpoint stiffness modifications during the catching experiment are shown in Figure 15. At the beginning of the experiment, a small constant increase in
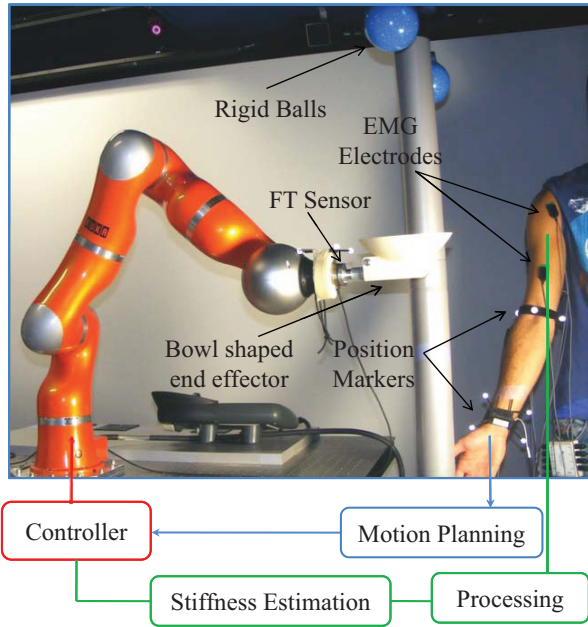
Fig. 11. Experimental setup of the ball-catching experiments. The slave KUKA LWR arm, EMG electrodes, position tracking markers and F/T sensor are shown.
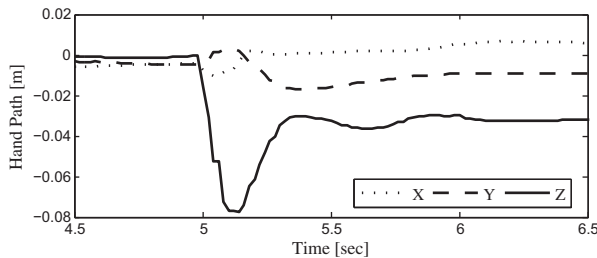

Fig. 12. Typical master's hand path in the *x*, *y* and *z* directions with respect to its initial position, and while performing the ball-reception task.
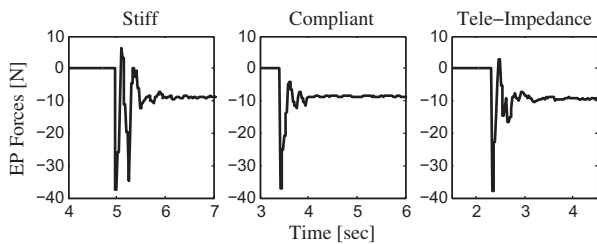

Fig. 13. Measured force values in the *z* direction during the task with the slave robotic arm under constantly high, constantly low, and tele-impedance stiffness control.

muscular activity could be observed, which led to relatively small increase in endpoint Cartesian stiffness values, compared with fully relaxed trials, which may refer to task readiness impedance tuning (Tsuji et al., 2004). Increased stiffness at the time of impact and its progressive decrease afterward are the results of explicit muscular activity regulation by the subject.
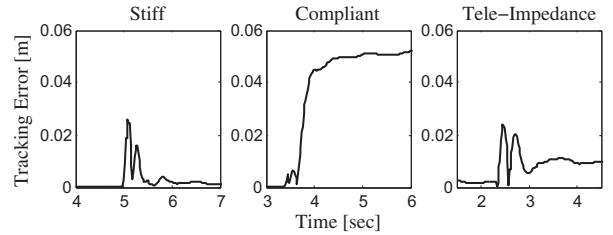

Fig. 14. Absolute tracking position error in the *z* direction during the task with the slave robotic arm under constantly high, constantly low, and tele-impedance stiffness control.
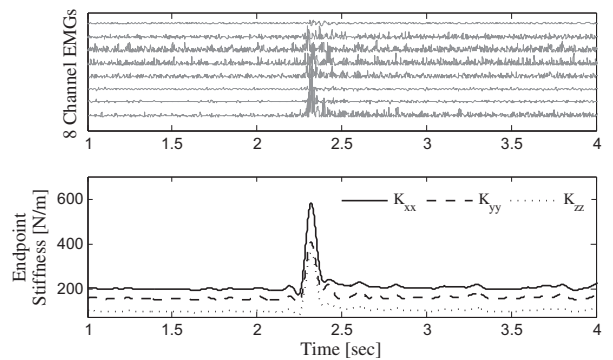

Fig. 15. Fully rectified eight-channel raw EMGs (upper plot) and estimated and mapped endpoint stiffness (lower plot) in real-time for the ball-reception task.

As could be expected, the stiffer the arm, the smaller the deviation is, as can be seen in the experimental results under constant high stiffness (Figure 14, left). The price paid for the accuracy and reduced deviation from equilibrium position with high values of endpoint stiffness is the occurrence of bouncing; indeed, the second force peak (at $t \approx 5.26$ s) in the stiff case (Figure 13, left) shows a second impact of the ball (see also Extension 1).

To obtain a more stable contact we need to reduce the endpoint stiffness values; however, using a constantly low stiffness directly affects the position deviation, which may reach very large, possibly unacceptable values (Figure 14, middle). Another drawback of such compliant control is the insufficiency of generated torques for repositioning the ball to its equilibrium even after transient end. The latter issue could be addressed by the master controlling his arm in a posture such as to compensate for the force of the slave, but this would cause a large discrepancy between the master and slave arm postures, affecting the intuitiveness of teleoperation.

The transient behavior of the system under tele-impedance appears to benefit from the active control of stiffness, increasing at the very first impact instants (from $t \approx 2.3$ s to $t \approx 2.4$ s), leading to a reduced deviation from the reference equilibrium position. Also, the bouncing phenomenon appears to be avoided thanks to the subsequent phase of stiffness reduction (between $t \approx 2.4$ s to $t \approx 2.7$ s,

see Figure 15). This behavior is in accordance with previous studies which have shown the capabilities of the human body to minimize soft-tissue vibrations and impact transitions by means of increased damping or decreased stiffness (modified resonance frequency) within involved tissues (see e.g. Wakeling et al., 2003). In addition, other behavioral studies demonstrated an increase of co-contraction levels in the human arm while performing tasks which need quick torque generations and/or to cancel components of torques orthogonal to the desired direction (Gribble et al., 2003).

To attempt a comparative analysis of performance in the ball reception task with the three control modes, we used three quantitative indices. The first index is computed as the integral of the difference between the vertical component of wrist force F_z and its steady-state value (i.e. the hand plus ball weight F_w) as

$$LOI = \int_{\Delta t} |f_z - f_w| \, dt, \qquad (8)$$

where δt is the time interval duration between the first impact and steady stabilization. A high value of the 'lift off index' *LOI* indicates a reception with multiple bouncing and/or long underdamped ball trajectories.

The second index is the maximum deviation from the equilibrium position in the z direction at steady state, evaluated as

$$PEI = max_{t \in \Delta t} |e_z|(t). \qquad (9)$$

A high value of the 'position error index' *PEI* indicates a reception where the slave arm is brought to postures too far from the master's.

As a third index, we consider an estimate of the damping ratio of the bouncing phenomenon, experimentally estimated (see e.g. Genta, 1995) using the logarithmic decrement between the first and second force peaks

$$\delta = \log \left(\frac{f_{z_{p,1}}}{f_{z_{p,2}}} \right)$$

as

$$DRI = \frac{1}{\sqrt{1 + \left(\frac{2\pi}{\delta} \right)^2}},$$

High values of the 'damping ratio index' *DRI* indicate the capability of the system to absorb energy and damp it quickly.

Fourth and finally, the 'bouncing time index' *BTI* was introduced as the duration of the interval during which contact between the ball and robot's end-effector is completely lost. The value is calculated by summing the intervals along which f_z is zero (complete disconnection) or positive (as result of acceleration of bowl) after the first impact.

Figure 16 shows the values obtained in experiments for the four indices in the three different stiffness regulation modes. Tele-impedance control apparently strikes a good compromise among the two extremes, consistently scoring close to the best performance obtained by either of the

two constant settings, thus enabling the human ability to be effectively transferred to the slave arm.

6. Conclusions

In this work the concept of tele-impedance was introduced, as a method to effectively transfer task-oriented stiffness control from the human master to the robotic slave arm. As an alternative to position-based or closed-loop bilateral force-reflecting teleoperation, the proposed approach enriches the command sent to the slave robot by combining the position reference with a stiffness (or full impedance) reference estimated from the arm of the human operator. The stiffness command to the robot was derived in real-time from the measurement of EMGs from eight muscles of the operator arm. A novel method was proposed for the estimation of stiffness in the human arm. This model was identified and calibrated through direct measurements of endpoint impedance. The procedures used for the calibration of the model were introduced and the tele-impedance control concept was illustrated through two complementary tasks. Although results obtained in this paper are encouraging, they have to be considered preliminary. Among the limitations of the present technique is the local validity of calibration data, and the need for recalibration in different poses and for different subjects. In addition, utilization of EMG signals in real environments suffers from some robustness issues. For instance, EMG signals are exposed to noise as results of cross talk and motion artifacts. Thermal and humidity variations might also give rise to EMG's variability, drift and inaccuracy. The need for recalibration as an outcome of subject-to-subject and day-to-day variations are other well-known disadvantages. Although in our experiments we found that the use of the same calibration data at relatively distant postures, and with other subjects than the person used for parameter estimation, was surprisingly effective, these were only anecdotal findings at this time, and the problem deserves much further work in the future.

Our approach to telemanipulation is unilateral in force, but requires visual feedback from the task scene. Although tele-impedance is intended to allow the user to control the robot forces indirectly through intuitively setting its stiffness, for particularly fragile environments (such as when the slave robot interacts with another human, or in surgery applications) this might not be enough, and it should be complemented with other means, e.g. simple augmented visual feedback giving indications about forces actually occurring at the interaction point.

The tele-impedance idea is to replicate in the robot whatever stiffness ellipsoid the human master uses. Our implementation and experiments show that indeed the method works, and tasks get done better than without tele-impedance control.

It is worth pointing out here that there is a classical literature in robot control that points out the advantages of
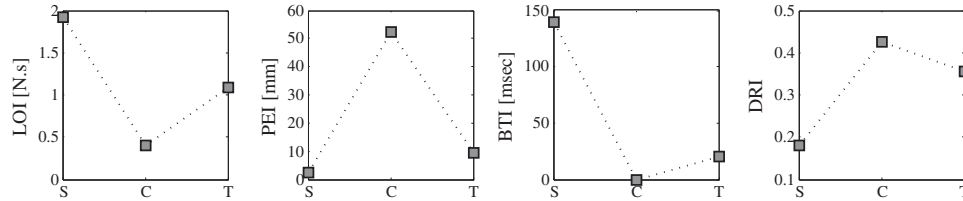
Fig. 16. Performance index plots over different elastic endpoint profiles (S, stiff; C, compliant; T, tele-impedance).

using Cartesian impedance control with different stiffness in different directions, e.g. for the peg-in-hole task (McCallion et al., 1979; Whitney and Rourke, 1986). There are also many results in neurophysiology which suggest that humans voluntarily orient their end-effector impedance ellipsoid using muscle co-contraction, in directions according to the task and/or the expected disturbances (Lacquaniti et al., 1993; Gomi and Osu, 1998; Burdet et al., 2001). However, there are also different views on the issue, such as (Perreault et al., 2002), who contend that 'individuals can voluntarily change stiffness orientation but the magnitude of these changes is small', and that 'endpoint force direction determines direction and magnitude of the stiffness orientations that can be achieved'.

However, as it can be noted from Figure 9 and especially from Figure 15, in our experiments the human subject's stiffness changes in the three directions were rather strongly correlated, suggesting that the subject might be controlling the size more than the shape of the stiffness ellipsoid in time during the different phases of the task. As a consequence, we do not have sufficient evidence to state that better performance is gained through replicating directional stiffness over a simpler, single-channel stiffness command.

Note

1. The existence of a right inverse is guaranteed by the fact that in nonsingular configurations T_F is full row-rank. Because $n > 3$, there exist infinite right-inverses: a particular choice is for instance $T_F^+ = T_F^{\mathrm{T}}(T_F T_F^{\mathrm{T}})^{-1}$, i.e. the pseudoinverse of T_F.

Funding

References

Adorno B, Bo A, Fraisse P and Poignet P (2011) Towards a cooperative framework for interactive manipulation involving a human and a humanoid. In *IEEE International Conference on Robotics and Automation*, pp. 3777–3783.

Akazawa K, Milner T and Stein R (1983) Modulation of reflex EMG and stiffness in response to stretch of human finger muscle. *Journal of Neurophisiology* 49: 16–27.

Albu-Schäffer A, Haddadin S, Ott C, Stemmer A, Wimbock T and Hirzinger G (2007b) The DLR lightweight robot lightweight design and soft robotics control concepts for robots in human environments. *Industrial Robot Journal* 34: 376–385.

Albu-Schäffer A, Ott C and Hirzinger G (2007a) A unified passivity-based control framework for position, torque and impedance control of flexible joint robots. *The International Journal of Robotics Research* 26: 23–39.

Artemiadis P and Kyriakopoulos K (2010) An EMG-based robot control scheme robust to time-varying EMG signal features. *IEEE Transactions on Information Technology in Biomedicine* 14: 582–588.

Bicchi A and Tonietti G (2004) Fast and soft arm tactics: Dealing with the safety-performance trade off in robot arms design and control. *IEEE Robotics and Automation Magazine* 11(2): 22–33.

Billard A and Grollman D (2011) Imitation learning (of robots). *Encyclopedia of the Sciences of Learning*. New York: Springer.

Burdet E, Osu R, Franklin D, Milner TE and Kawato M (2001) The central nervous system stabilizes unstable dynamics by learning optimal impedance. *Nature* 414: 446–449.

Castellini C and Van Der Smagt P (2009) Surface EMG in advanced hand prothetics. *Biological Cybernetics* 100: 35–47.

De Serres S and Milner T (1991) Wrist muscle activation patterns and stiffness associated with stable and unstable mechanical loads. *Experimental Brain Research* 86: 451–458.

Dolan J, Friedman M and Nagurka M (1993) Dynamic and loaded impedance components in the maintenance of human arm posture. *IEEE Transactions on Systems, Man, and Cybernetics* 23: 698–709.

Eusebi A and Melchiorri C (1998) Force reflecting telemanipulators with timedelay: Stability analysis and control design. *IEEE Transactions on Robotics and Automation* 14: 635–640.

Franklin D, Osu R, Burdet E, Kawato M and Milner T (2003) Adaptation to stable and unstable dynamics achieved by combined impedance control and inverse dynamics model. *Journal of Neurophysiology* 90: 3270–3282.

Fukuda O, Tsuji T, Kaneko M and Otsuka A (2003) A human-assisting manipulator teleoperated by EMG signals and arm motions. *IEEE Transactions on Robotics and Automation* 19: 210–222.

Genta G (1995) *Vibration of Structures and Machines*. New York: Springer-Verlag.

Goertz R, Blomgren R, Grimson J, Forster G, Thompson W and Kline W (1961) The ANL model 3 master–slave electric manipulator - its design and use in a cave. *Transactions of the American Nuclear Society* 4: 219–220.

Gomi H and Osu R (1998) Task-dependent viscoelasticity of human multi joint arm and its spatial characteristics for interaction with environments. *Journal of Neuroscience* 18: 65–78.

Gribble P, Mullin L, Cothros N and Mattar A (2003) Role of cocontraction in arm movement accuracy. *Journal of Neurophysiology* 89: 2396–2405.

Gribble P and Ostry D (2000) Compensation for loads during arm movements using equilibrium-point control. *Experimental Brain Research* 135: 474–482.

Gulrez T, Tognetti A, Fishbach A, et al. (2008) Controlling wheelchairs by body motions: A learning framework for the adaptive remapping of space. In *International Conference on Cognitive Systems*.

Hannaford B and Anderson R (1988) Experimental and simulation studies of hard contact in force reflecting teleoperation. In *International Conference on Robotics and Automation*, pp. 584–589.

Howard M, Braun D and Vijayakumar S (2011) Constraint based equilibrium and stiffness control of variable stiffness actuators. In *IEEE Conference on Robotics and Automation (ICRA)*.

Imaida T, Yokokohji Y, Doi T, Oda M and Yoshikawa T (2004) Ground space bilateral teleoperation of ETS-VII robot arm by direct bilateral coupling under 7-s time delay condition. *IEEE Transactions on Robotics and Automation* 20: 499–511.

Jafari A, Tsagarakis N, Vanderborght B and Caldwell D (2011) A new variable stiffness actuator (CompAct-VSA): Design and modelling. In *IEEE/RSJ International Conference on Intelligent Robots and Systems (IROS)*, pp. 378–384.

Kawato M (1999) Internal models for motor control and trajectory planning. *Current Opinion in Neurobiology* 9: 718–727.

Lacquaniti F, Carrozzo M and Borghese N (1993) Time–varying mechanical behavior of multijointed arm in man. *Journal of Neurophysiology* 69: 1443–1463.

Leung G, Francis B and Apkarian J (1995) Bilateral controller for teleoperators with time delay via mu-synthesis. *IEEE Transactions on Robotics and Automation*.

Mann K, Werner F and Palmer A (1989) Frequency spectrum analysis of wrist motion for activities of daily living. *Journal of Orthopaedic research* 7: 304–306.

McCallion H, Johnson G and Pham D (1979) A compliant device for inserting a peg in a hole. *Industrial Robot: An International Journal* 6(2): 81–87.

Millan J, Renkens F, Mourino J and Gerstner W (2004) Non-invasive brain-actuated control of a mobile robot by human EEG. *IEEE Transactions on Biomedical Engineering* 51: 1026–1033.

Milner T (2002) Contribution of geometry and joint stiffness to mechanical stability of the human arm. *Experimental Brain Research* 143: 515–519.

Milner T, Cloutier C, Leger A and Franklin D (1995) Inability to activate muscle maximally during cocontraction and the effect on joint stiffness. *Experimental Brain Research* 107: 293–305.

Mussa-Ivaldi F, Hogan N and Bizzi E (1985) Neural, mechanical, and geometric factors subserving arm posture in humans. *Journal of Neuroscience* 5: 2732–2743.

Mussa-Ivaldi F and Miller L (2003) Brain-machine interfaces: Computational demands and clinical needs meet basic neuroscience. *Trends in Neuroscience* 26: 329–334.

Niemeyer G and Slotine J (2004) Telemanipulation with time delays. *The International Journal of Robotics Research* 23: 873–890.

Osu R, Franklin D, Kato H, et al. (2002) Short- and long-term changes in joint co-contraction associated with motor learning as revealed from surface EMG. *Journal of Neurophysiology* 88: 991–1004.

Osu R and Gomi H (1999) Multijoint muscle regulation mechanism examined by measured human arm stiffness and EMG signals. *Journal of Neurophysiology* 81: 1458–1468.

Perreault E, Kirsch R and Crago P (2002) Voluntary control of static endpoint stiffness during force regulation tasks. *Journal of Neurophysiology* 87: 2808–2816.

Perreault E, Kirsch R and Crago P (2004) Multijoint dynamics and postural stability of the human arm. *Experimental Brain Research* 157: 507–517.

Schreiber G, Stemmer A and Bischoff R (2010) The fast research interface for the Kuka lightweight robot. In *IEEE Conference on Robotics and Automation (ICRA)*.

Selen L, Beek P and Dieen JV (2005) Can co-activation reduce kinematic variability? A simulation study. *Biological Cybernetics* 93: 373–381.

Sheridan T (1993) Space teleoperation through time delay: Review and prognosis. *IEEE Transactions on Robotics and Automation* 9: 592–606.

Shin D, Kim J and Koike Y (2009) A myokinetic arm model for estimating joint torque and stiffness from EMG signals during maintained posture. *Journal of Neurophisiology* 101: 387–401.

Tee K, Burdet E, Chew C and Milner T (2004) A model of force and impedance in human arm movements. *Biological Cybernetics* 90: 368–375.

Tonietti G, Schiavi R and Bicchi A (2005) Design and control of a variable stiffness actuator for safe and fast physical human/robot interaction. In *IEEE International Conference on Robotics and Automation*, pp. 526–531.

Trumbower R, Krutky M, Yang B and Perreault E (2009) Use of self-selected postures to regulate multijoint stiffness during unconstrained tasks. *PLoS One* 4(5).

Tsuji T, Morasso P, Goto K and Ito K (1995) Human hand impedance characteristics during maintained posture. *Biological Cybernetics* 72: 475–485.

Tsuji T, Takeda Y and Tanaka Y (2004) Analysis of mechanical impedance in human arm movements using a virtual tennis system. *Biological Cybernetics* 91: 295–305.

Turvey M (2007) Action and perception at the level of synergies. *Human Movement Science* 26: 657–697.

Vogel J, Castellini C and Der Smagt P (2011) EMG-based teleoperation and manipulation with the DLR LWR-III): Design and modelling. In *IEEE/RSJ International Conference on Intelligent Robots and Systems (IROS)*, pp. 672–678.

Wakeling J, Liphardt A and Nigg B (2003) Muscle activity reduces soft-tissue resonance at heel-strike during walking. *Journal of Biomechanics* 36: 1761–1769.

Weiss P (1941) *The Self-differentiation of the Basic Patterns of Coordination*. Baltimore, MD: The Williams & Wilkins Company.

Whitney D and Rourke J (1986) Mechanical behavior and design equations for elastomer shear pad remote center compliances. *Journal of Dynamic Systems, Measurement, and Control* 108: 223–232.

Appendix: Index to Multimedia Extensions

The multimedia extension page is found at http://www.ijrr.org

Table of Multimedia Extensions

Extension	Type	Description
1	Video	Peg-in-hole and ball-reception experiments